doi:10.1016/j.jmb.2007.08.063 J. Mol. Biol. (2007) 373, 1305–1320

JMB

Available online at www.sciencedirect.com

ScienceDirect

ELSEVIER

Tracing Changes in Protonation: A Prerequisite to Factorize Thermodynamic Data of Inhibitor Binding to Aldose Reductase

Holger Steuber, Paul Czodrowski, Christoph A. Sotriffer and Gerhard Klebe*

Department of Pharmaceutical Chemistry, Philipps-University Marburg, Marbacher Weg 6 35032 Marburg, Germany

Received 24 March 2007; received in revised form 25 August 2007; accepted 29 August 2007
Available online
5 September 2007

To prevent diabetic complications derived from enhanced glucose flux *via* the polyol pathway the development of aldose reductase inhibitors (ARIs) has been established as a promising therapeutic concept. Here, we study the binding process of inhibitors to aldose reductase (ALR2) with respect to changes of the protonation inventory upon complex formation. Knowledge of such processes is a prerequisite to factorize the binding free energy into enthalpic and entropic contributions on an absolute scale. Our isothermal titration calorimetry (ITC) measurements suggest a proton uptake upon complex formation with carboxylate-type inhibitors. As the protonation event will contribute strongly to the enthalpic signal recorded during ITC experiments, knowledge about the proton-accepting and releasing functional groups of the system is of utmost importance. However, this is intricate to retrieve, if, as in the present case, both, binding site and ligand possess several titratable groups. Here, we present pK_a calculations complemented by mutagenesis and thermodynamic measurements suggesting a tyrosine residue located in the catalytic site (Tyr48) as a likely candidate to act as proton acceptor upon inhibitor binding, as it occurs deprotonated to a remarkable extent if only the cofactor $NADP^+$ is bound. We furthermore provide evidence that the protonation state and binding thermodynamics depend strongly on the oxidation state of the cofactor`s nicotinamide moiety. Binding thermodynamics of IDD 388, IDD 393, tolrestat, sorbinil, and fidarestat are discussed in the context of substituent effects.

Keywords: structure-based drug design; protonation state; pK_a calculation; thermodynamic driving forces; aldose reductase

Edited by J. E. Ladbury

Introduction

Bio-molecular recognition involves the formation of non-covalent interactions that govern biological processes such as substrate binding and conversion by enzymes, or the assembly of protein–protein and protein–ligand complexes.[1] Crystal structure analysis provides detailed insights into the spatial arrangement of such complexes, whereas isothermal titration calorimetry (ITC) elucidates the thermodynamic properties of the binding process. The Gibbs free energy of binding (ΔG^0) can be factorized into enthalpic (ΔH^0) and entropic ($-T\Delta S^0$) contributions to unravel the driving forces of complex formation.[2–5] They can be dominated by an enthalpic or entropic contribution. In due course of ligand optimization, the strategies to be followed can be rather different depending on whether an enthalpic or entropic driving force should be amplified. It has been suggested, that ligands optimized for enthalpic reasons can better escape resistance development caused by rapid mutagenesis of e.g. a viral target

*Corresponding author. E-mail address: klebe@staff.uni-marburg.de.

Abbreviations used: ALR1, aldehyde reductase; ALR2, aldose reductase; WT, wild-type; PB calculation, Poisson–Boltzmann calculation; PEOE, partial equalization of orbital electronegativities; K_b, binding constant; ITC, isothermal titration calorimetry.

protein.[6,7] In contrast, it can only be speculated that selectivity discrimination among multiple protein isoforms would require perfect protein–ligand shape complementarity usually paralleled by a pronounced optimization of entropic binding factors, e.g. by chemically arresting the ligand in its bioactive conformation, thereby reducing the conformational entropic penalty upon complex formation. One important contribution to binding is given by hydrogen bonds formed between functional groups of the ligand and the protein. Depending on their protonation states different types of interactions and strengths will be formed. Particularly, if protonation or deprotonation creates charged species, significant contributions to binding affinity can occur. If the pK_a value of a functional group falls next to the pH of the applied buffer conditions, partial protonation will occur. Such groups are referred to as "titratable groups". Their protonation state depends on the local environment determining the distribution of charges and, in consequence, the adopted pK_a value. Protonation states of titratable groups are difficult to determine. The resolution of protein crystal structures is usually not sufficient to allow for an unambiguous assignment of protonation states. The situation becomes even more complicated by the fact that the accommodation of a ligand may change the local electrostatics in the binding pocket as well and, accordingly, modulate the *pKa* values.[8]

In consequence, changes of protonation states of ligand and protein functional groups will occur upon ligand binding. They complicate the assignment of H-bond donor or acceptor properties.[9] Furthermore, the interpretation of ITC measurements is affected by such changes: the experimentally observed heat signal comprises, besides the binding enthalpy, also all ionization enthalpies resulting from the transfer of protons between buffer components, ligand molecules, and titratable protein functional groups. Thus, before a meaningful factorization of the measured binding free energy (ΔG^0) into enthalpic and entropic contributions can be performed, all superimposed contributions from proton transfer reactions have to be subtracted from the measured heat signal.[5,9,10]

Here we report on the application of ITC measurements combined with a mutagenesis approach and Poisson–Boltzmann (PB) calculations to trace changes in protonation states induced upon inhibitor binding to the enzyme human aldose reductase (EC 1.1.1.21) (ALR2). These observations are subsequently exploited to factorize the binding free energy into enthalpic and entropic contributions.

Human aldose reductase is a 36 kDa $(\beta/\alpha)_8$-TIM-barrel folded aldo-keto reductase. It is the first enzyme of the polyol pathway and converts various aldehydes to their corresponding non-reactive alcohols using NADPH as the reducing cofactor. The latter donates a hydride ion to the carbonyl carbon of the aldehyde, most likely followed by a subsequent proton transfer from one of the neighbouring acidic protein residues placed next to the intermediate substrate anion.[15,16] Along the polyol pathway, ALR2 is of pathophysiological relevance. Under elevated blood glucose levels, present in patients suffering from diabetes mellitus, it converts a remarkable extent of glucose to sorbitol.[17] The latter is subsequently oxidized to fructose by the NAD^+-dependent sorbitol dehydrogenase, the second enzyme of the polyol pathway. Accordingly, increased flux of glucose *via* the polyol pathway leads to various biochemical imbalances such as osmotic and oxidative stress, pathological interferences with kinase cascades, apoptotic regulation, and cytokine signalling, altogether resulting in diabetic long-term complications.[18–21] Thus, the

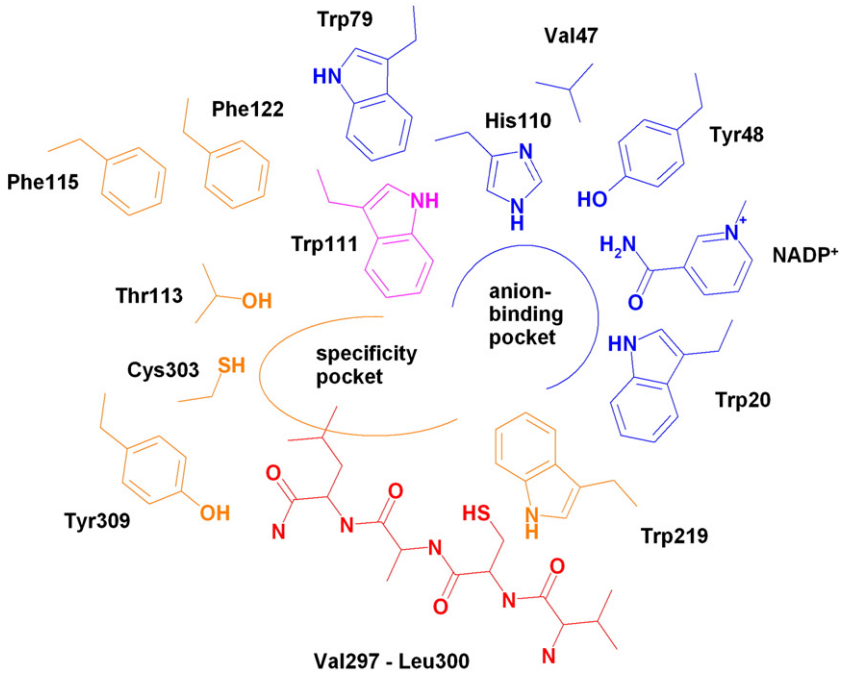

Figure 1. Schematic representation of the ALR2 binding pocket.[46] The catalytic site is represented in blue, the specificity pocket in orange. Amino acids exhibiting high mobility throughout several crystal structures are shown in red. Trp111 dividing the entire binding pocket into the two sub-pockets is shown in magenta.

development of ALR2-inhibitors (ARIs) has been proven to be a promising therapeutic concept.

The active site of ALR2 is located at the C-terminal region of the enzyme. The binding pocket is divided by Trp111 into the catalytic and the specificity subpocket. The latter shows distinct conformational adaptations depending on the bound ligand. The deeply buried substrate binding pocket comprises residues presumably participating in the catalytic reaction mechanism (Tyr48, Lys77, His110), the nicotinamide moiety of NADP+, and Trp111 which forms *via* its indole NH group an H-bond to most of the described ligand head groups. Further hydrophobic contacts can be formed by the side-chains Trp20, Val47, Trp79, and Trp219 (Figure 1). This catalytic cavity is usually addressed by hydrophilic, negatively charged functional groups of the ligands. Decorated at the opposing end with appropriate hydrophobic groups, these ligands can provoke pronounced "induced-fit" adaptations. A specificity pocket is formed by different rotameric states of Ala299, Leu300, and Phe122 at the solvent exposed site and by the side-chain of Trp111 facing the protein interior.[11–14]

In order to study the driving forces of inhibitor binding, particularly with respect to the superimposed induced-fit adaptations, we performed ITC measurements paralleled with PB calculations to identify changes in protonation states upon ligand binding. After correction of the superimposed ionization steps we factorized the binding free energy into enthalpic and entropic contributions.

Results and Discussion

Analysis of changes of the protonation inventory upon ligand binding

A detailed assignment of protonation states of the titratable groups after complex formation with a carboxylate-type inhibitor has been performed based on the 0.66 Å resolution ALR2–IDD 594 complex structure (**1**, Figure 2).[11] The titratable groups of

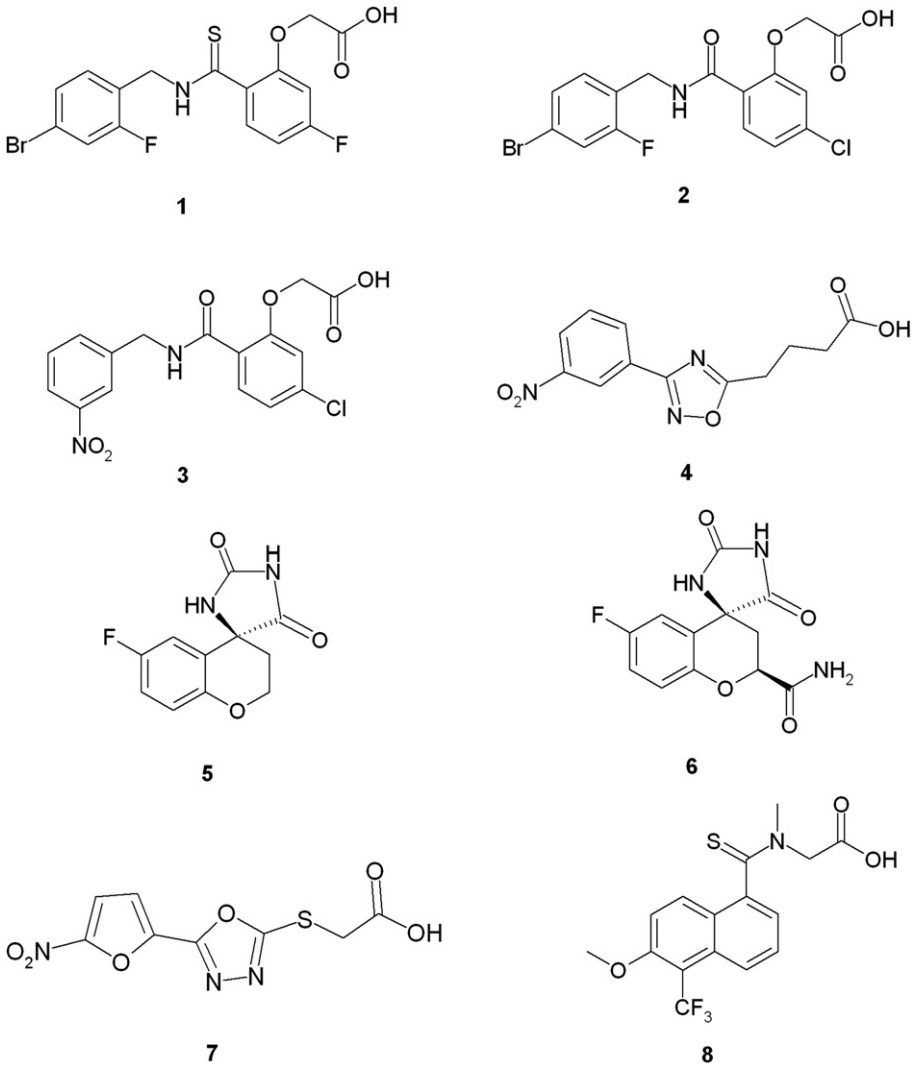

Figure 2. Chemical formulae of the studied aldose reductase inhibitors: **1,** IDD 594; **2,** IDD 388; **3,** IDD 393; **4** and **7,** lead compounds obtained by virtual screening; **5,** sorbinil; **6,** fidatestat; **8,** tolrestat.

interest comprise the carboxylate function of the inhibitor and the side-chains of Asp43, Tyr48, Lys77, and His110. The difference electron density in this ultra-high resolution structure suggests the carboxylate of IDD 594 (**1**, Figure 2) to bind deprotonated. *Via* its oxygen O1 it accepts an H-bond from Trp111 $N^{\varepsilon 1}$ (3.1 Å). Oxygen O2 forms H-bonds to Tyr48 OH (O-H bond vector pointing towards O2) and His110 $N^{\varepsilon 2}$ (2.7 Å; Figure 3). Interestingly, the histidine is singly protonated at $N^{\varepsilon 2}$, the second nitrogen $N^{\delta 1}$ accepts an H-bond from a neighbouring water molecule (2.9 Å). This geometry is further confirmed by neutron diffraction experiments based on single crystals produced from the fully deuterated protein. The negatively charged carboxylate of IDD 594 performs an electrostatic interaction with the positively charged nicotinamide ring of the cofactor (3.4 Å). Tyr48 OH accepts a hydrogen bond from Lys77 NZ, which is threefold protonated. In addition, Lys77 is involved in a salt bridge to Asp43 (2.7 Å and 3.4 Å between NZ and the carboxylate oxygen atoms of Asp43).

Although the protonation states are well characterized after ligand binding, no comparable information is available for the uncomplexed holo-enzyme. To trace possible changes, we performed ITC measurements in four buffers of different ionization enthalpies. As the experimentally observed heat signal ΔH^0_{exp} comprises the binding enthalpy ΔH^0_{bind} and the contribution resulting from the ionization of buffer molecules, a putative

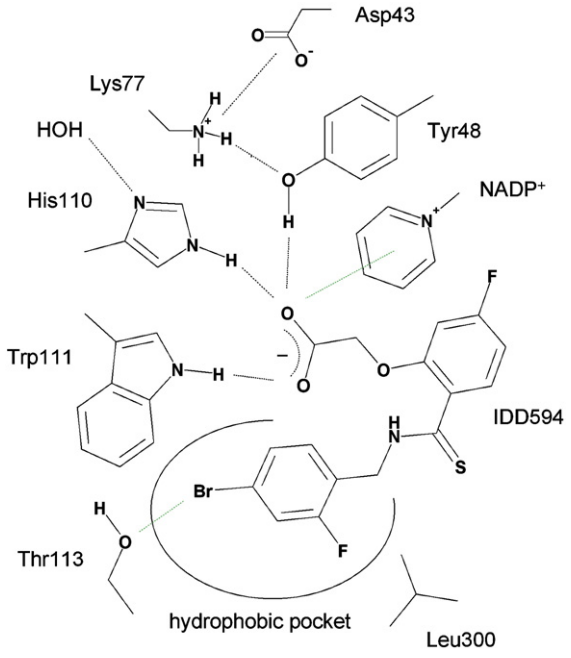

Figure 3. Schematic representation of the ALR2 binding pocket complexed with IDD 594 (**1**). The Figure indicates the protonation states of the titratable residues as observed in the 0.66 Å resolution structure. Hydrogen bonds (black) and other polar contacts (green) are depicted as broken lines.

net proton uptake or release will be superimposed in the recorded heat signal ΔH^0_{exp} (equation (1)):[5,10]

$$\Delta H^0_{exp} = \Delta H^0_{bind} + nH^0_{ion,buffer} \quad (1)$$

Three carboxylate-type inhibitors, **2**, **3**, and **4**, were studied (Figure 2): IDD 388 (**2**) exhibits a virtually identical constitution as IDD 594 (**1**) and places its carboxylate moiety almost exactly in the same position as IDD 594. Accordingly, protonation states of protein and ligand after binding to ALR2 can be assumed to be identical for inhibitors **1** and **2**. The same is valid for IDD 393 (**3**), which is equipped with a meta-nitrophenyl moiety instead of a halogenated aromatic terminus. Inhibitor **4** was identified by virtual screening.[22] Its carboxylate group binds to the catalytic site by picking up an interstitial water molecule which mediates an interaction to Trp111.[23] This is accompanied by a shift of the carboxylate towards Tyr48 resulting in hydrogen bonds to the latter (2.4 Å) and to His110 $N^{\varepsilon 2}$ (2.5 Å; Figure 4). These structural deviations and putative changes of the local dielectricity caused by the incorporated water molecule revealed inhibitor **4** as an interesting candidate for the analysis of protonation state changes.

The positive slope of the linear regression (Figure 5) fitting ΔH^0_{exp} *versus* $H^0_{ion,buffer}$ at pH 8 in the presence of $NADP^+$ indicates a proton uptake upon complex formation with **2**, **3**, and **4**. In molar ratio, 0.8(±0.2) mol of protons are picked-up upon binding of inhibitor **2**, and 0.9(±0.2) mol upon binding of inhibitor **3**. Despite deviations in the carboxylate binding geometry, ALR2–**4** exhibits a comparable proton uptake of 0.8(±0.1) mol of protons. The low pK_a values of the studied carboxylate-type inhibitors (Table 4, below), suggest their carboxylate groups as almost completely dissociated in aqueous solution. Thus, the proton pick-up derives from deprotonation of the buffer molecules resulting in the ΔH^0_{exp} *versus* $H^0_{ion,buffer}$ dependency.

As mentioned, the high-resolution ALR2–IDD 594 complex suggests Tyr48 OH, Lys77 NZ, and His110 $N^{\varepsilon 2}$ to be in protonated state, and the ligand`s carboxylate in deprotonated situation. Thus, the question remains which titratable residue is responsible for the proton uptake recorded by our ITC measurements. As prior to factorization an appropriate correction for the ionization enthalpy of the involved functional group has to be performed to reveal the net ΔH^0_{bind}, this issue is of utmost importance. As neither sufficiently resolved crystal structures or neutron structures, nor NMR data for the uncomplexed holo-enzyme are available, we consulted pK_a calculations considering the crucial titratable active site functional groups. We used the PB solver MEAD[24] based on our recently developed partial equalization of orbital electronegativities (PEOE)_PB charge model.[9]

We started from the complexed crystal structures of ALR2 and removed inhibitors **2**–**4** from their binding sites to investigate the resulting pK_a shifts. The analysis of ligand-deleted structures is a very

pragmatic approach, as the geometry for the uncomplexed protein is generated by simply removing the three ligands from the complex neglecting putative adaptations of the binding cavity upon removal of the ligand. However, we applied this approach successfully for other examples.[25,26] The influence of the dielectric constant by using different values ($\varepsilon_{protein}$ = 10 or 20) and the impact of the orientation of the conformationally flexible Tyr48 OH group with respect to its pK_a value were studied (Table 1). A general review on the application of the PB method is given by Baker.[27] One particular open and unresolved issue in continuum electrostatics calculations is the choice of the dielectric constant ($\varepsilon_{Protein}$). The interested reader is referred to Warshel's review on this topic.[28] Nonetheless, we will mention several studies to outline the broad range of values applied for $\varepsilon_{Protein}$: Antosiewicz *et al.* used a value of 20 in their studies.[29] Demchuk & Wade differentiated between solvent-exposed ($\varepsilon_{Protein}$ of 80) and desolvated residues ($\varepsilon_{Protein}$ of 15) in their PB-based pK_a calculations,[30] whereas Nielsen & McCammon employed a single value of 8 for all residues.[31] In our computations on the protonation effects in HIV protease,[26] we were able to achieve better agreement with experiment while using an

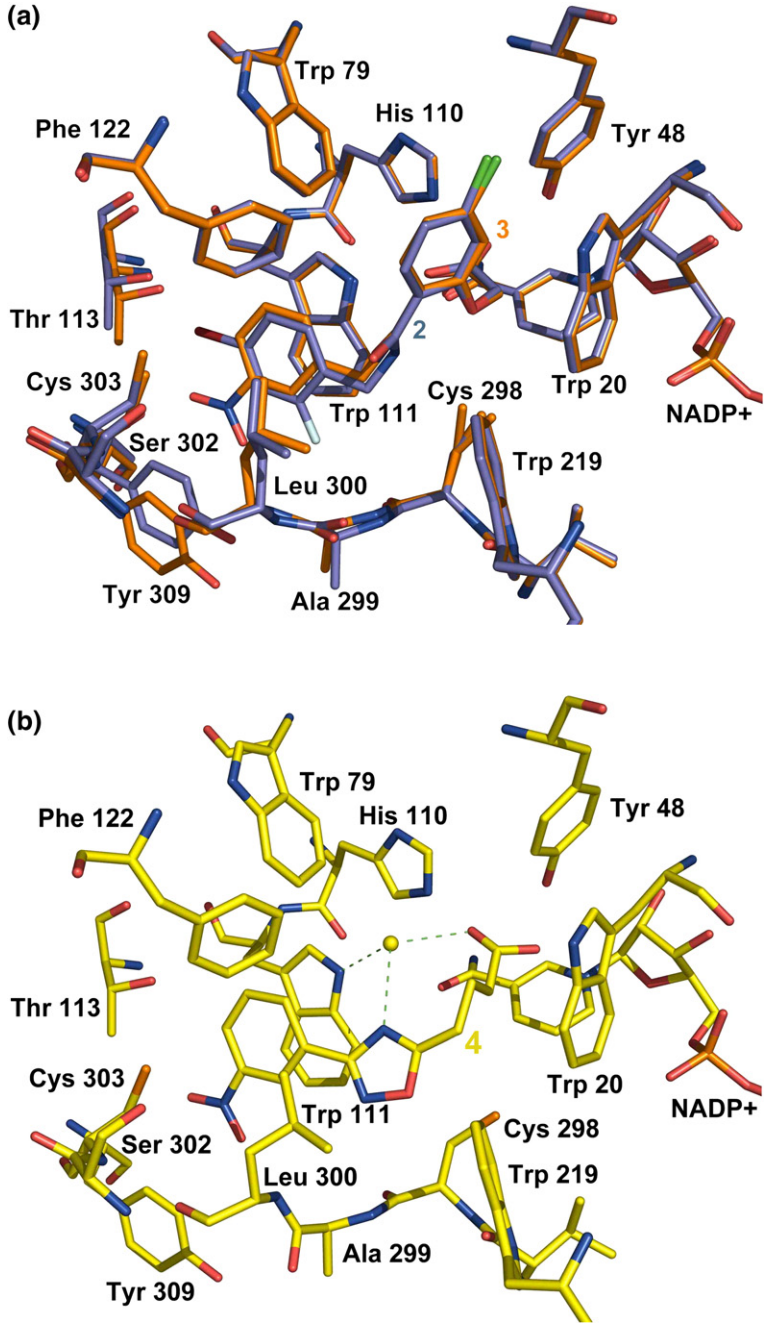

Figure 4. Binding mode of the ALR2 inhibitors **2** (blue), **3** (orange, superimposed in (a)), and **4** (yellow, shown in (b)). The interstitial water molecule only present in the ALR2–**4** complex is shown as yellow sphere.

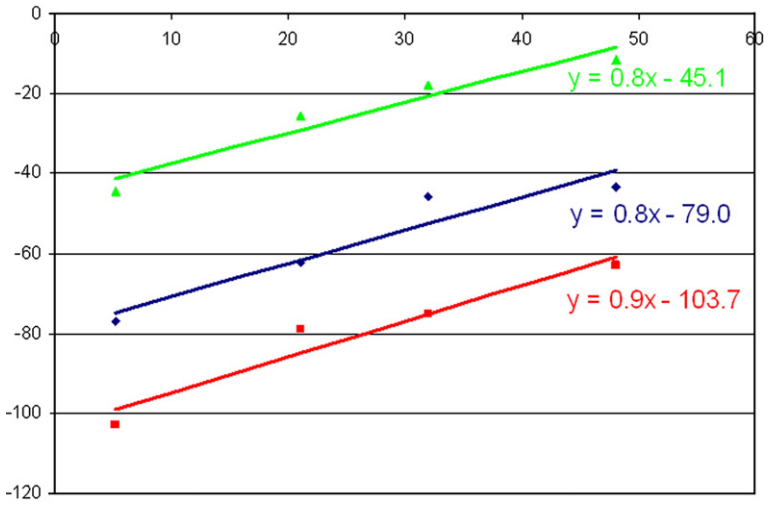

Figure 5. ΔH^0_{exp} (y, in kJ mol^{-1}) *versus* $\Delta H^0_{ion,buffer}$ (x, in kJ mol^{-1}) plots for the carboxylate-type inhibitors **2** (blue), **3** (red), and **4** (green) titrated to WT ALR2 in the presence of NADP$^+$. The positive slope represents the proton uptake of the protein–ligand complex upon binding.

$\varepsilon_{Protein}$ value of 10. Obviously, no generally applicable value for the protein dielectric constant has yet been defined.

In a further example, xylanase, we were able to describe a pronounced influence of the Tyr80 OH orientation on the pK_a value of an active site glutamate.[9] In ALR2, the two Tyr48 OH orientations shown in Figure 6 were considered for all three ligand-deleted structures. The estimated pK_a values for Tyr48 and His110 are given in Tables 1 and 2, respectively. For His110, N$^{\delta1}$ has been defined as sole titratable group. This setting considers the fact that N$^{\varepsilon2}$ is involved in a direct hydrogen bond to the ligand. For the remaining titratable residues of the active site, Asp43 and Lys77, no pK_a values suggesting strong shifts from the standard values were observed and they are, hence, not listed in the Tables.

The orientation of the Tyr48 OH-group shows a remarkable influence. Choosing the orientation towards Asp43 and a dielectric constant of 10 reveals a mean pK_a value of 6.29, which corresponds to virtually full deprotonation (Table 1) in the uncomplexed state. For His110, rather low pK_a values are suggested indicating an uncharged, singly protonated state of this residue (Table 2). The calculations for the protein residues considered in the ligand-bound state are listed in Table 3. They suggest, in agreement with the crystallographic results, that the carboxylic group of the ligand remains deprotonated. Furthermore, the calculations indicate a strong pK_a shift for Tyr48 towards basic values, whereas the values for His110 remain in the acidic range. These findings suggest, in agreement with crystallographic evidence, that Tyr48 acts as proton acceptor upon complexation and adopts a neutral state in the ligand-bound situation. In contrast, His110 does not experience comparably strong pK_a shifts and remains uncharged upon ligand complexation. Considering the value for Tyr48 before complexation (4% protonation, $\varepsilon = 10$) a net uptake of $n_{calc} = 0.96$ mol of protons is suggested. This value is in good agreement with experiment. The pK_a calculations performed for $\varepsilon = 20$ suggest a similar trend, even though agreement with experimental data is less satisfactory.

Likely, our calculations overestimate the upward pK_a shift of Tyr48, but the trends are suggested correctly. For the ligand-deleted ALR2–**2** crystal structure, variants to the standard settings were examined: (a) the explicit consideration of one water molecule which donates a hydrogen bond from beyond the catalytic site to the N$^{\delta1}$ atom of His110; (b) the titration of His110 N$^{\varepsilon2}$ instead of N$^{\delta1}$. The effect of the explicit inclusion of the water molecule is rather marginal, it modulates the values by less than 0.1 pK_a unit for Tyr48. Also switching to N$^{\varepsilon2}$ as titratable group of His110 results in pK_a values for

Table 1. Calculated pK_a values for Tyr48 OH of the uncomplexed holo-enzyme (cofactor considered in oxidized state)

Tyr48 OH towards	ε	**2**	**3**	**4**	Mean (std. Dev.)
Asp43	10	5.82	6.27	6.79	6.29 (0.49)
His110	10	8.45	8.52	9.09	8.69 (0.35)
Asp43	20	7.70	7.84	8.15	7.90 (0.23)
His110	20	8.72	8.78	9.13	8.88 (0.22)

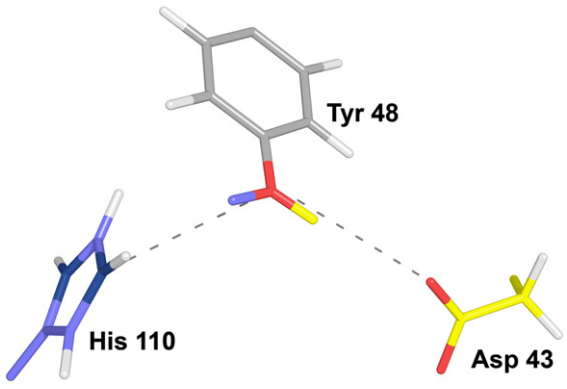

Figure 6. The two orientations studied of the Tyr48 OH group: it is either oriented towards Asp43 (yellow) or His110 (blue).

Table 2. Calculated pK_a values for His110 N^{δ} of the uncomplexed holo-enzyme (cofactor considered in oxidized state)

Tyr48 OH towards	ε	**2**	**3**	**4**	Mean (std. Dev.)
Asp43	10	−1.40	−1.70	−1.47	−1.52 (0.16)
His110	10	−1.75	−2.02	−1.80	−1.86 (0.14)
Asp43	20	2.34	2.07	2.36	2.26 (0.16)
His110	20	1.97	1.78	2.02	1.92 (0.13)

Tyr48 which deviate by only 0.5 log unit (predicting a higher pK_a value for Tyr48 compared to the $N^{\delta 1}$ titration).

At first glance, our computational results suggest Tyr48 OH as likely candidate for proton acceptance. This premise appears rather surprising in light of the fact that residues such as histidine, aspartate or lysine are in close neighbourhood, which are usually assumed to be responsible for protonation effects in catalytic sites. Nevertheless, the computer simulations prompted us to perform mutagenesis of Tyr48 to phenylalanine (Y48F). Although kinetic measurements revealed that this mutant is catalytically inactive[32] inhibitor binding should be accessible by ITC. As the affinity of $NADP^+$ is virtually not influenced by the mutation ($K_{b(WT,\ NADP^+)}$ 6.3(±0.7)×10^5 l mol^{-1}; $K_{b(Y48F,\ NADP^+)}$ 8.9(±0.1)×10^5 l mol^{-1}), putative changes of the protonation inventory observed for Y48F cannot be provoked by a different cofactor binding behaviour or altered population in the pocket. Table 4 summarizes the experimentally observed net change of the protonation inventory for wild-type ALR2 (WT). Indeed, repetition of our ITC experiments with Y48F showed no buffer dependence (n = 0.0±0.1) upon binding of **2** (Figure 7, dark blue). In agreement with our pK_a calculations, these experimental results suggest the phenolic oxygen of Tyr48 as the proton acceptor. Accordingly, in the $NADP^+$ bound state at pH 8, this residue is obviously deprotonated to about 80% and becomes fully protonated upon inhibitor binding. Otherwise, the crystallographically observed hydrogen bond between the ligand`s carboxylate group and Tyr48 OH could not be established. Possibly, the negative charge of the deprotonated tyrosine in the holo-enzyme compensates to some extent the positive charge of the nicotinamide moiety of the oxidized cofactor (3.2 Å between Tyr48 OH and C2 of $NADP^+$) in absence of a ligand. This compensation will not be given in the uncomplexed Y48F mutant. Obviously, the electrostatic properties of the cofactor strongly influence the protonation state of Tyr48 OH. These considerations prompted us to repeat the binding study of inhibitor **2** with the reduced cofactor NADPH (Figure 7, light blue). Now, for the same ligand a proton uptake of 0.2(±0.04) mol is observed, suggesting Tyr48 OH to be 80% protonated in the uncomplexed NADPH-bound state. Assuming a 1:1 stoichiometry for inhibitor binding, these 0.2 mol of protons would be required to fully protonate Tyr48 OH. These observations are in agreement with pH-dependent kinetic measurements,[33] suggesting (for the C298A mutant) a Tyr48 OH pK_a value of 7.6 for the $NADP^+$-bound and 8.25 for the WT–NADPH-bound state. Based on these findings, at pH 8 Tyr48 should be deprotonated to 72% in the presence of $NADP^+$, and to 36% once NADPH is bound. However, these pK_a estimations derived from kinetic experiments are to some degree substrate-dependent. In consequence, they do not exactly match with our thermodynamic evaluation.

Besides carboxylate-type inhibitors such as **1**–**4**, the hydantoins sorbinil (**5**) and its more potent derivative fidarestat (**6**) are well known inhibitors of ALR2. They exhibit strongly deviating pK_a values in water compared to the carboxylate-type inhibitors (fidarestat: 7.9, sorbinil: 8.4). Accordingly, 55.8% of inhibitor **6** are deprotonated at pH 8 prior to binding. Our ITC experiments indicate a net uptake of 0.3(±0.1) mol of protons per mol of bound inhibitor upon ALR2–**6** complexation in the presence of $NADP^+$ (Figure 7, red). Following the assumption that Tyr48 is to 80% deprotonated in the uncomplexed holo-enzyme, this net proton pick-up results from the superposition of the full protonation of Tyr48 upon complexation and the release of 0.5 mol of protons by inhibitor **6,** which is about 50% protonated in solution and binds to the protein as deprotonated hydantoin. In this negatively charged state it accepts charge-assisted hydrogen bonds from His110 $N^{\varepsilon 2}$ and Tyr48 OH. This hypothesis is strongly supported by the fact that under the same conditions inhibitor **6** binds to Y48F with a release of 0.5(±0.1) mol of protons per mol of bound ligand (Figure 7, orange). As the phenolic oxygen of Tyr48 is missing in Y48F the entire protonation effect can be attributed to the proton release of the ligand (50% protonated) to the buffer.

Replacing $NADP^+$ by its reduced form under otherwise unchanged conditions results in a net release of n = −0.3±0.05 for the WT protein (Figure 7, yellow). Assuming Tyr48 OH to be 80% protonated in the NADPH-bound holo-state, this net inventory can be factorized into a release of 0.5 mol of protons from the partially protonated inhibitor **6** superimposed by an uptake of 0.2 mol of protons by the 20% deprotonated Tyr48 OH to achieve full protonation.

A similar interpretation can be performed for the hydantoin sorbinil (**5**). According to its pK_a value (8.4), at pH 8 the ligand is to 71% protonated in aqueous solution. Assuming full deprotonation of the hydantoin upon complexation along with an uptake of 0.8 mol of protons by Tyr48 should mutually compensate to a net pick-up of about 0.1

Table 3. Calculated pK_a values for Tyr48 and His110 of the complexed enzyme (cofactor considered in oxidized state)

	2 pK_a		**3** pK_a		**4** pK_a		
ε	Tyr48	His110	Tyr48	His110	Tyr48	His110	n_{calc}
10	16.15	1.92	17.16	1.61	31.10	2.54	+0.96
20	13.67	5.48	14.37	5.14	16.33	5.60	+0.51

Table 4. Overview of protonation effects occurring upon ligand binding

	2 (IDD388)		**3** (IDD393)	**4**	**5** (sorbinil)		**6** (fidarestat)	
	$NADP^+$	NADPH	$NADP^+$	$NADP^+$	$NADP^+$	NADPH	$NADP^+$	NADPH
Ligand pK_a value	2.8	2.8	2.8	4.3	8.4	8.4	7.9	7.9
Neutral fraction of inhibitor prior to binding (%)[a]	~0	~0	~0	~0	71	71	44	44
Net change of protonation inventory (WT)[b] (mol /mol complex)	0.8	0.2	0.9	0.8	0.1	−0.5	0.3	−0.3
Suggested proton uptake by Tyr48 OH (WT) (mol / mol complex)	0.8	0.2	0.9	0.8	0.8	0.2	0.8	0.2

[a] The neutral fraction of inhibitor has been calculated according to the Henderson–Hasselbalch equation.
[b] The net change of the protonation inventory for wild-type (WT) was observed experimentally; based on these results a proton uptake by the deprotonated fraction of Tyr48 OH is suggested.

mol of protons in the presence of $NADP^+$. Indeed, for inhibitor **5** we observe an experimental net change of 0.1(±0.02) mol of protons (Figure 7, dark green).

In the presence of NADPH, where only about 0.2 mol of protons per mol of bound inhibitor are picked up by Tyr48 OH, a net release of approximately $n=-0.5$ mol protons should be expected. The experimental value of −0.5(±0.2) mol protons (Figure 7, light green) matches well with this interpretation.

The computationally predicted role of Tyr48 as a proton acceptor is in good agreement with experimental evidence, suggesting untypical protonation effects of the tyrosine residue. Similar effects have been described in literature, e.g. for dTDP-glucose 4,6-dehydratase,[34] UDP-galactose 4-epimerase,[35] and human glutathione transferase A1-1.[36] For dTDP-glucose 4,6-dehydratase, a pKa shift of Tyr160 to a value of 6.41 has been observed by kinetic measurements.[34] The resulting tyrosyl anion is stabilized by neighbouring lysine and threonine residues which enable this tyrosine residue to act as a putative base in the catalytic mechanism. A similar constellation has been described for UDP-galactose 4-epimerase with a resulting pK_a value of 6.1 for the tyrosine moiety.[35] A further example is given by Tyr9 in human glutathione transferase A1-1, which displays a pK_a value of 8.1.[36] In this context, the partially deprotonated character of the tyrosine presumably contributes to an activation of the glutathione thiol group by establishment of a hydrogen bond, thereby stabilizing its deprotonated (nucleophilic) form.

Factorization into enthalpic and entropic contributions

In order to factorize the free energy of binding, the standard binding enthalpy ΔH^0_{bind} has to be determined based on the original heat signal ΔH^0_{exp} observed from the ITC experiment. According to

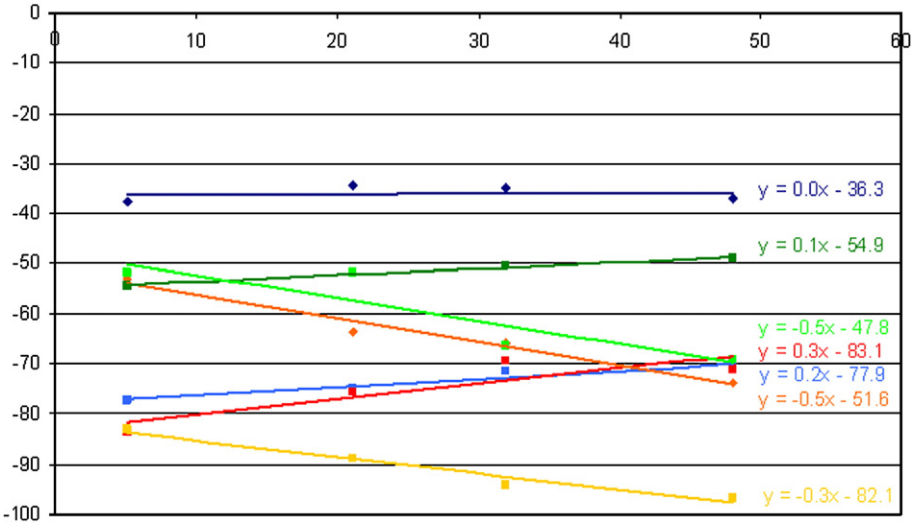

Figure 7. ΔH^0_{exp} (y, in kJ mol^{-1}) *versus* $\Delta H^0_{ion,buffer}$ (x, in kJ mol^{-1}) plots for the titration of inhibitors **2**, **5**, and **6** to ALR2 WT and Y48F mutant in the presence of $NADP^+$ or NADPH. The slope indicates the net proton transfer. Titrations to the WT enzyme are represented (■), titrations to Y48F are also shown (♦). The titration of inhibitor **2** to Y48F in the presence of $NADP^+$ is shown in dark blue, the one of **2** to WT ALR2 is represented in light blue. Titrations of inhibitor **5** to ALR2 in the presence of $NADP^+$ and NADPH are shown in dark green and light green, respectively. The results for inhibitor **6** titrated to ALR2 in the presence of $NADP^+$ are given in red, those in the presence of NADPH are shown in yellow, and those for Y48F in presence of $NADP^+$ are represented in orange.

Table 5. Net contributions for the protonation of functional groups in buffer, protein and ligand

	Cofactor	Ligand	n_1 (buffer contribution)	n_2 (protein contribution)	n_3 (ligand contribution)
WT	NADP+	**2, 4**	0.8	−0.8	0
		3	0.9	−0.9	0
		5	0.1	−0.8	0.7
		6	0.3	−0.8	0.5
	NADPH	**2**	0.2	−0.2	0
		5	−0.5	−0.2	0.7
		6	−0.3	−0.2	0.5
Y48F	NADP+	**2**	0	0	0
		6	−0.5	0	0.5
	NADPH	**2**	0	0	0

Values of n_1, n_2, and n_3 are listed for the ligands studied under differing oxidation state of the cofactor for both WT and Y48F. These values were used for the calculation of ΔH^0_{bind} according to equation (2).

equation (2), the following contributions superimpose with ΔH^0_{bind}:

$$\Delta H^0_{\text{exp}} = \Delta H^0_{\text{bind}} + n_1 H^0_{\text{ion,buffer}} + n_2 H^0_{\text{ion,protein}} + n_3 H^0_{\text{ion,ligand}} \quad (2)$$

Values used for n_1, n_2, and n_3 are listed in Table 5. The entropic contribution $-T\Delta S^0$ has been calculated as the difference between ΔG^0 and ΔH^0_{bind} according to the Gibbs–Helmholz equation.

Correlation of thermodynamic and structural features

The mutation Y48F was initially performed to confirm Tyr48 as atypically protonated residue predicted by our pK_a calculations. In addition, the thermodynamic analysis reveals the energetic contribution of the Tyr48 OH – ligand hydrogen bond to binding affinity. Two types of anchor groups, carboxylate (**2**) and hydantoin (**6**), have been studied for WT and Y48F binding. Table 6 lists the original heat signal (ΔH^0_{exp}) together with the corrected values (ΔH^0_{bind}) for the different ligands, with respect to WT ALR2 and Y48F. The cofactor is considered in oxidized and reduced state. Interestingly, binding of the carboxylate-type inhibitor **2** appears to be more affected ($\Delta\,\Delta G^0 \sim 8.5$ kJ mol^{-1}) by the loss of the Tyr48 OH H-bond compared to the hydantoin (**6**) ($\Delta\,\Delta G^0 \sim 1.4$ kJ mol^{-1}). Assuming a similar architecture for both complexes, WT and Y48F, inhibitor **6** is obviously better capable to compensate for the loss of the hydrogen bond, possibly by gradually increasing the strength of the remaining contacts to His110 $N^{\varepsilon 2}$ and Trp111 $N^{\varepsilon 1}$. This is also reflected by the standard binding enthalpies: the mutational loss of the Tyr48 OH group is paralleled by a 23 kJ mol^{-1} reduced binding enthalpy for inhibitor **2**, whereas inhibitor **6** experiences only half of this amount ($\Delta\,\Delta H^0_{\text{bind}} \sim 11.5$ kJ mol^{-1}). Both, inhibitors **2** and **6** show a more favourable entropic contribution for Y48F compared to WT ($-T(\Delta\,\Delta S^0)$(**2**) 14.2 kJ mol^{-1}, $-T(\Delta\,\Delta S^0)$(**6**) 10.1 kJ mol^{-1}). This might result from an entropically favourable higher residual mobility of the Phe48 side-chain (and possibly other residues) as a consequence of the Tyr48 OH group loss as this residue maintains the hydrogen-bond network between Asp43, Lys77 and His110 in the WT.

The replacement of $NADP^+$ by its reduced form decreases the free energy of binding by 2–3 kJ mol^{-1} as shown for inhibitors **2**, **5**, and **6**. This drop possibly occurs due to the reduced electrostatic interactions between the negatively charged ligand anchor group and the either positively charged or neutral nicotinamide ring of $NADP^+$ or NADPH,

Table 6. Thermodynamic parameters of the studied inhibitors

		K_b (10^6 l mol^{-1})	ΔG^0 (kJ mol^{-1})	ΔH^0_{exp} (kJ mol^{-1})	ΔH^0_{bind} (kJ mol^{-1})	$-T\Delta S^0$ (kJ mol^{-1})
WT, NADP+	**2**	31.5±8.5	−42.7±3.1	−79.0±5.9	−59.0±5.9	16.3±9.0
	3	25.0±4.1	−42.2±0.8	−103.7±5.0	−81.2±5.0	39.0±5.8
	4	1.65±0.34	−35.4±1.0	−45.1±4.4	−25.1±4.4	−10.3±5.4
	5	4.5±0.6	−37.9±0.7	−54.9±0.6	−54.7±0.7	16.8±1.4
	6	153.0±36.6	−46.7±1.2	−83.1±3.7	−79.5±4.0	32.8±5.2
	7	0.31±0.1	−31.3±1.6	−8.7±1.0	−5.6±1.0	−25.7±2.6
	8	4.6±1.2	−38.0±1.3	−34.1±0.8	−31.0±0.8	−7.0±2.1
WT, NADPH	**2**	13.3±2.0	−40.6±0.8	−77.9±1.2	−72.9±1.2	32.3±2.0
	5	1.3±0.2	−34.9±0.7	−47.8±5.1	−62.6±5.6	27.7±6.3
	6	61.7±15.9	−44.4±1.3	−82.1±1.5	−93.5±1.7	49.1±3.0
Y48F, NADP+	**2**	1.0±0.2	−34.2±1.0	−36.3±1.5	−36.3±1.5	2.1±2.5
	6	86.9±16.5	−45.3±0.9	−51.6±1.7	−68.0±2.0	22.7±2.9
Y48F, NADPH	**2**	0.16±0.04	−29.7±1.2	−39.6±1.9	−39.6±1.9	9.9±3.1

The ionization enthalpy of the tyrosine side-chain (Tyr48) used for the correction of the binding enthalpy was obtained from M. Chaplin [http://www.sbu.ac.uk/biology/enztech/ph.html].

respectively. Surprisingly, our factorization suggests a more favourable enthalpic contribution ΔH^0_{bind} for inhibitor binding to the NADPH-bound enzyme compared to the oxidized state (inhibitor **5**: ~8 kJ mol^{-1}, inhibitors **2** and **6**: ~14 kJ mol^{-1}). At first glance, this is unexpected, as a loss of electrostatic interactions is assumed to be accompanied by a loss in binding enthalpy. However, the present case might be more complex. The positive charge on the nicotinamide moiety $NADP^+$ compared to the neutral system of NADPH will polarize the neighbouring groups involved in hydrogen bonding. This redistribution of charges can alter the strength of such hydrogen bonds[37,38] resulting in an overall enthalpic advantage with the cofactor in the reduced state. The hypothesis of an enthalpically more favourable hydrogen bond network involving the carboxylate group of, e.g. inhibitor **2** in the presence of NADPH compared to $NADP^+$ is also reflected by the binding thermodynamics to Y48F. In the mutant, the hydrogen bond to Tyr48 cannot be established. In presence of $NADP^+$, the binding enthalpy drops by 22.7 kJ mol^{-1} in consequence of the mutation, whereas in the presence of NADPH the corresponding drop in binding enthalpy amounts to 33.3 kJ mol^{-1}.This indicates that the H-bond loss in presence of NADPH demands an even larger enthalpic penalty. Overall, the difference in ΔG^0_{bind} of 8.5 kJ mol^{-1} for WT–**2** and Y48F–**2** with bound $NADP^+$ indicates a ΔG^0_{bind} contribution for the hydrogen bond. The corresponding pair in the reduced state indicates a slightly larger value of 10.9 kJ mol^{-1}. The affinity difference for binding of inhibitor **2** to the oxidized and reduced cofactor present in WT or Y48F amounts to 2.1 or 4.5 kJ mol^{-1}, respectively.

In order to analyse the deviating thermodynamic profiles, ΔG^0, ΔH^0_{bind}, and $-T\Delta S^0$ are shown in Figure 8 for the $NADP^+$-bound WT enzyme. Two representatives of the IDD series (**2** and **3**), two ligands identified by a virtual screening campaign (**4** and **7**), tolrestat (**8**) and two hydantoins (**5** and **6**) are studied.

Comparing the thermodynamic profiles of ligands sharing the same scaffold, a meaningful correlation between substituent patterns and thermodynamic driving forces becomes apparent. Whereas in inhibitor **2** the terminal phenyl ring bears an ortho-fluoro and a para-bromo substituent, in inhibitor **3** a meta-nitro group is present. The binding modes of inhibitors **2** and **3** are displayed in Figure 4. The aromatic portions of both ligands occupy the specificity pocket. Inhibitor **2** forms an electrostatic interaction between its bromo substituent and the side-chain oxygen of Thr113. In contrast to the latter complex, inhibitor **3** induces structural changes in the Ala299–Leu300 peptide region, thus facilitating hydrogen bond formation between Leu300 NH and one of the nitro oxygen atoms. Furthermore, the side-chain of Tyr309 is shifted and the nitro group accepts two non-classical hydrogen bonds from the aromatic dipolar C-H groups of Tyr309.[23] This is obviously accompanied by a more favourable enthalpic contribution (~22 kJ mol^{-1}) paralleled by a compensating entropic penalty. The latter might be the price that has to be paid due to a more pronounced spatial arrest of the ligand provoked by these additional interactions and the required adaptations of the protein. Despite this deviating thermodynamic factorization, both ligands share a virtually identical free energy of binding.

The ligands **4** and **7** (Figure 2) both possess a terminal nitro-aromatic tail linked to an oxadiazole ring, which is further connected by a two or three-membered alkyl spacer to the carboxylate anchor group. Even though both share a similar overall topology, their thermodynamic profiles differ remarkably. In contrast to the pairs **2**,**3** and **5**,**6**, their binding is favoured by either enthalpic and entropic contributions, nevertheless to varying extent. Inhibitor **4** picks up a water molecule mediating the hydrogen bond between its carboxylate and Trp111 $N^{\varepsilon 1}$. Furthermore, it exhibits one additional rotatable bond compared to inhibitor **7** and, thus, becomes likely more restrained upon binding compared to its solvated state. The incorporation of a water molecule is enthalpically favourable and entropically unfavourable. Furthermore, the immobilization of one additional rotatable bond in inhibitor **4** should be detrimental entropically. Therefore, binding of inhibitor **7** shows an entropic advantage compared to **4**. Both ligands, **4**

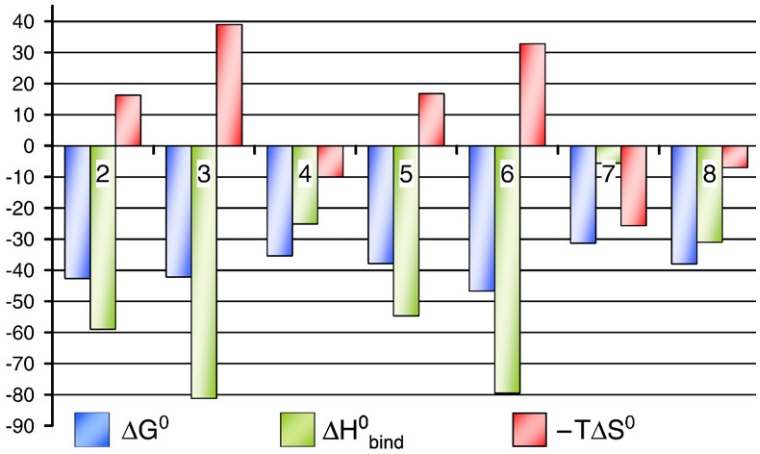

Figure 8. Bar diagram of the standard free energies of binding (blue) and its factorization into enthalpic (green) and entropic (red) contributions for the inhibitors **2**–**8** in the presence of $NADP^+$. All values are given in kJ mol^{-1}.

and **7**, possess an oxadiazole ring with deviating topology. In the ALR2–**4** complex, the oxygen and one nitrogen are saturated by polar contacts to the sulphur atom of Cys298 (3.5 Å) and the interstitial water molecule (2.8 Å), respectively. However, none of the hetero-atoms in the oxadiazole of inhibitor **7** finds appropriate binding partners. In addition, inhibitor **7** possesses a furan ring as terminal aromatic moiety and a sulphur atom incorporated into the aliphatic spacer. Also these hetero-atoms are poorly saturated by polar contacts in the complex, as only the sulphur atom forms a weak hydrogen bond to a bulk water (3.5 Å). These polar hetero-atoms, which remain unsaturated in the complex contribute enthalpically unfavourable, as they implicate an imbalanced solvation/desolvation inventory. In summary, for inhibitor **7** more polar groups remain unsatisfied compared to **4,** resulting in a ~4 kJ mol^{-1} reduced binding affinity. Likely, also in case of inhibitor **4** the replacement of non-saturated heteroatoms would improve the enthalpic binding contribution.

The carboxylate-type inhibitor tolrestat (**8**) possesses a similar thermodynamic profile as inhibitor **4**, with a 6 kJ mol^{-1} more favourable binding enthalpy and a 3 kJ mol^{-1} less favourable entropic contribution resulting in a 3 kJ mol^{-1} more favourable ΔG^0. This observation is to some extent surprising, as inhibitor **8** does not pick up a water molecule upon complex formation and exhibits a more rigid skeleton. However, it induces a distinct protein binding pocket conformer up to now only observed for inhibitor **8** and adopts a different binding geometry. Besides polar contacts involving the carboxylate head group, a hydrogen bond between Ser302 O^{γ} and one fluorine atom of the ligand is formed (2.9 Å). A comparison of the non-polar surface buried upon binding of inhibitors **4** and **8** reveals that in the latter complex about 150 Å^2 additional non-polar surface area is buried, whereas in ALR2–**4** about 50 Å^2 additional polar surface are removed (ALR2–**4**: buried polar surface: 240.3 Å^2, buried apolar surface: 373.2 Å^2; ALR2–**8**: buried polar surface 187.2 Å^2, buried non-polar surface 519.7 Å^2). Due to the different protein conformations induced by accommodation of both ligands, the thermodynamic data are difficult to compare. The more enthalpic binding of inhibitor **8** compared to **4** could possibly be explained by a more favourable desolvation of inhibitor **8** following the concept of the "non-classical hydrophobic effect".[39]

In contrast to all other inhibitors studied in this contribution the hydantoins **5** and **6** exhibit a different anchor group and bind to ALR2 keeping the specificity pocket in closed state (Figure 9).[13,40,41] Both ligands share an identical scaffold. In addition, inhibitor **6** possesses an exocyclic amide group, which forms a direct H-bond to the Leu300 NH group (3.0 Å). Ligand **5** also establishes a contact to the Leu300 NH group, however, mediated *via* an interstitial water molecule picked up upon complex formation. The presence of the exocyclic amide function in inhibitor **6** is obviously attributed to a gain in binding free energy of 8.8 kJ mol^{-1} (Table 6). The free energy of binding factorizes into a 25 kJ mol^{-1} more favourable enthalpy of inhibitor **6** over **5**, and an entropic advantage of **5** ($-T\Delta\ \Delta S^0$ 16 kJ mol^{-1}). The enthalpic gain of inhibitor **6** can presumably be attributed to the formation of a direct H-bond to the protein which results in an entropically less favourable arrest of either the ligand and the C-terminal loop of the protein. As mentioned above, the pick up of a water molecule should be enthalpically favourable and entropically unfavourable. In both complexes, ALR2–**5** and ALR2–**6**, the ligands are associated with a water molecule (Figure 9). Thus, at first glance, the thermodynamic inventory due to water incorporation should be balanced. However, the water molecule observed in ALR2–**6** mediates an intra-ligand H-bond between its ether oxygen and the amide nitrogen (3.2 Å), presumably also present in the uncomplexed state. In case of inhibitor **5**, the H-bond is only mediated through a water molecule, and this contact might be enthalpically of comparable strength to the situation in water. Furthermore, the special arrest of protein and ligand reinforced by a water-mediated contact might be less pronounced compared to the situation observed for inhibitor **6**, revealing a residual entropic benefit for inhibitor **5**.

Ligands **3** and **6** exhibit deviating scaffolds and induce different adaptations to the protein. Both show strong enthalpic binding paralleled by a pronounced entropic penalty of almost equal size. The matching thermodynamic profiles are particularly surprising as they bind to the enzyme either in the specificity pocket-closed or opened state. Assuming that no intricate and mutually compensating effects are in operation, this observation suggests the energy barrier between open and closed state to be rather small. Possibly, water takes a significant influence on the opening process. In the non-crystalline phase the dynamic properties of the C-terminal loop region might allow the specificity pocket to adopt an open conformation, which is in due course filled by water molecules demanding an entropic penalty. Subsequent desolvation of the partly hydrophobic pocket upon ligand binding could compensate to some extent for the entropic penalty along with enthalpy contributions required for the opening process.

Conclusions

Here, we investigated the binding thermodynamics of different aldose reductase inhibitors to better understand the driving forces of ligand binding in the light of their adopted binding modes. However, prior to any meaningful factorization of the free energy of binding into enthalpic and entropic contributions, a detailed analysis of putative changes in the protonation inventory is required to correct for any superimposed heat contributions resulting from ionization effects. By means of ITC measurements we were able to detect an uptake

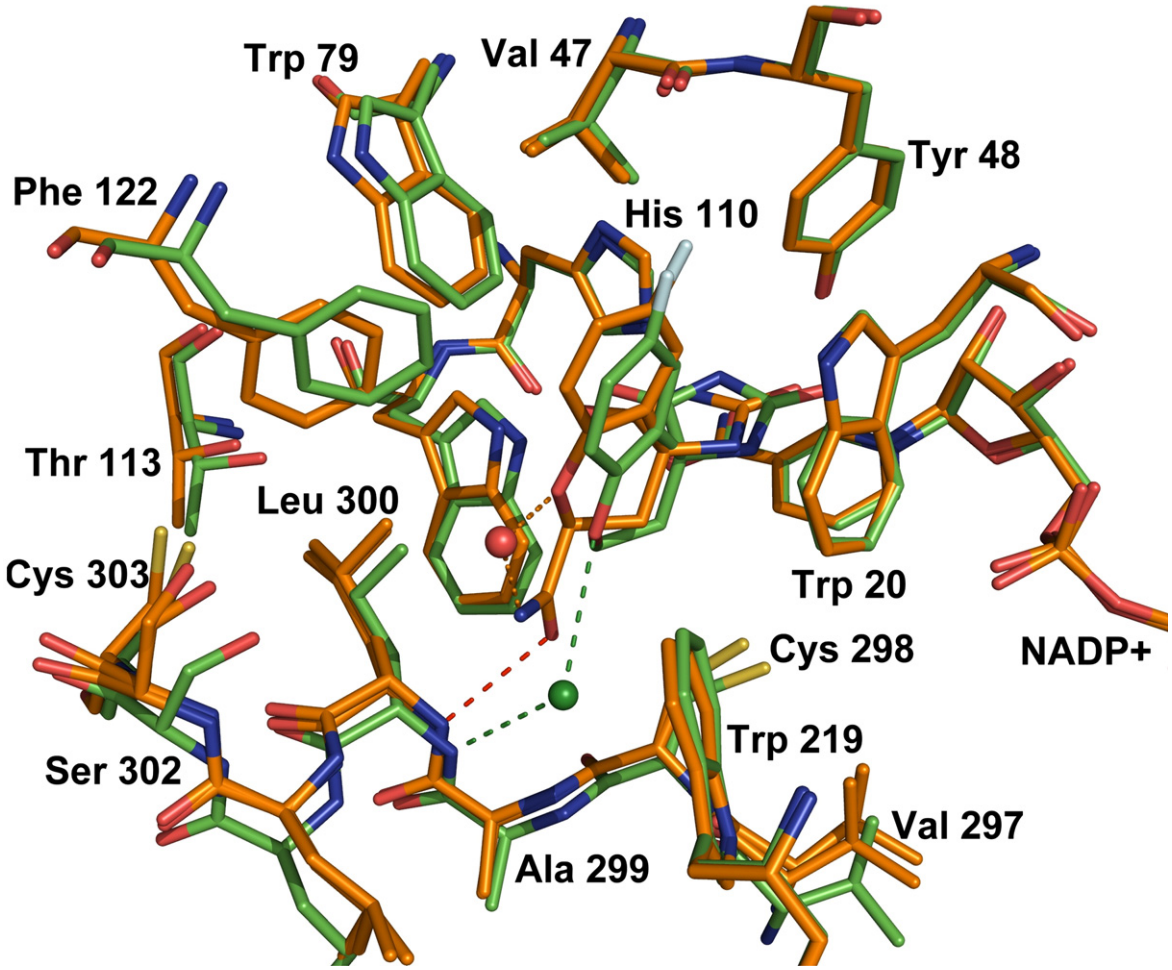

Figure 9. Superposition of the ALR2 binding pocket complexed with inhibitor **5** (green), and inhibitor **6** (orange). The interstitial water molecule only present in the ALR2–**5** complex is shown in green, whereas the water captured by fidarestat is in red. Corresponding H-bonds are shown as broken lines. The hydrogen bond directly formed between the amide group of fidarestat (**6**) and Leu300 NH is shown in red.

of approximately 0.8 mol of protons per mol of formed complex upon binding of carboxylate-type inhibitors to the enzyme with the cofactor in the oxidized state. Several titratable groups are present in the catalytic pocket that might pick up this proton. As the likely candidates for proton acceptance (e.g. Lys77 instead of Tyr48) show strongly deviating heats of ionization, correct assignment is essential (e.g. Tyr OH: 25 kJ mol^{-1}; Lys NZ: 45 kJ mol^{-1})†. We performed PB-based pK_a calculations using our PEOE_PB charge model, recently developed in our laboratory.[9] This computational approach suggested Tyr48 as a likely proton acceptor. Subsequently, this could be confirmed experimentally by mutating Tyr48 to Phe. Binding of carboxylate-type inhibitors to the mutant leads to the absence of any buffer-dependent proton transfer. On the contrary, hydantoins, partially protonated prior to binding, release their protons whereas Tyr48 picks-up a similar amount as observed for the carboxylate-type inhibitors. In agreement with computational prediction the experimental results provide evidence for Tyr48 as a proton acceptor. This interpretation follows the most simple model; however, a more complex scenario cannot be fully excluded. The neighbouring titratable residues could also experience a pK_a shift in response to the mutation of Tyr to Phe, thereby pretending an overall equilibrated proton balance for the Phe mutant. Even though this constellation cannot be completely rejected, we suppose this situation as rather unlikely. The amino group of Lys77 is most likely protonated as it will experience an increased pK_a value due to the short-distant electrostatic contacts to the neighbouring negatively charged Asp43. The latter residue is observed as deprotonated in sufficiently resolved crystal structures. Thus, it is not available as a putative candidate for proton acceptance upon ligand binding. If His110 would be the proton acceptor upon ligand binding, Tyr48 would have to lower the pK_a of His110 in a drastic way, so that it would bear a negative charge state prior to ligand binding. It would then adopt a neutral state after ligand binding. This neutral state

†Chaplin, M. (2002). http://www.sbu.ac.uk/biology/enztech/ph.html

of His110 subsequent to ligand binding has been confirmed by the detected hydrogen atoms in the 0.66 Å resolved ALR2–IDD594 crystal structure[11] and neutron diffraction experiments[42] on the same complex. Thus, Tyr48 remains as the most likely candidate for proton acceptance, which is in full agreement with our mutational and computational results.

Our measurements suggest that the protonation inventory and the binding thermodynamics depend strongly on the oxidation state of the cofactor. This knowledge is essential in order to apply appropriate corrections of the superimposed ionization contributions. It further indicates that the energetics of the hydrogen bonds formed between the ligand anchor group and the catalytic site residues are dependent on the oxidation state. Such properties might be essential for the accommodation of substrate and release of product along a reaction pathway.

Our factorization into enthalpic and entropic contributions suffers to some degree from the limitation that the ionization enthalpies of protein and ligand titratable groups, used for the correction have been determined in aqueous solution. A different chemical environment as the enzyme active site will affect these values to some extent and, thus, could influence the accuracy of the results. In principle, the shift of pK_a values and deviations in the ionization enthalpy of functional groups experienced upon ligand binding can be assessed experimentally by ITC measurements at various pH values in order to obtain a sufficient amount of data for global fitting of the unknown variables as described, e.g. for elastase, endothiapepsin, and plasmepsin II.[10,43–45] Nevertheless, the present system experiences solubility limitations that restrict the required broad range pH variations. Furthermore, significant pH changes will likely alter the protonation states of other protein and ligand titratable groups, along with their ionization enthalpies in the bound and unbound state. Thus, in our study we decided to discuss relative differences in a series of related ligands based on standard values of ionization enthalpies determined in aqueous solution. Most likely, the local effects will be of similar magnitude for all complexes studied.

The factorization indicates the influence of different substituents attached to a given ligand scaffold on the thermodynamic binding profile. For example, an imbalanced inventory of polar ligand atoms which do not find appropriate polar contacts within the complex are penalized by an unfavourable desolvation enthalpy. This is detrimental to the binding enthalpy and should be avoided.

Entropic contributions are more difficult to interpret, particularly, if only limited information about the dynamic properties of ligand and protein prior to and after binding is available. Recent NMR studies of ligand binding to major urinary protein (MUP)[1] suggested changes of ordering parameters of protein residues partly remote from the actual binding site. Such changes of the residual entropy are essentially difficult to predict and to interpret if only the crystal structure of a protein–ligand complex is available. However, these contributions can take strong influence towards the entropic term, particularly, if they are affected by the complexation. In the case of adaptive proteins such as ALR2, it is in question, how much energy is required to transform the enzyme between different pocket conformers. Such knowledge would presumably be helpful to estimate whether binding affinity of a given ligand scaffold will profit from the decoration with appropriate groups opening sub-pockets of the protein. A comparison of the thermodynamic profiles observed for inhibitors **3** and **6** suggests that the energetic barrier which separates the open from the closed specificity pocket is rather low, as postulated earlier on the basis of molecular dynamics simulations.[46] These properties likely determine the accommodation of substrates and agree with the broad substrate promiscuity of ALR2.

Materials and Methods

Compounds **4** (BTB02809) and **7** (JFD00882) were purchased from Chempur, Karlsruhe, Germany. Expression and purification of aldose reductase have been described.[11–13] The mutation of tyrosine 48 to phenylalanine was introduced by PCR, using the Pfu Turbo polymerase (Stratagene), to amplify the entire plasmid. In order to construct the mutant, the primer with the following sequence was obtained from MWG-Biotech (Ebersberg, Germany): 5′- CCTCATTCTCATTCTGGAACACATGGGCACAGTCGATGTGG – 3′. After 20 cycles of PCR, the initial plasmid was digested by DpnI enzyme for 30 min at 37 °C. After amplification (in XL2 Blue *Escherichia coli* strain), purification with the Quiagen Miniprep kit and sequencing (MWG-Biotech) to confirm the mutation, the mutated plasmid was transformed into the *E. coli* strain BL21 Gold for protein production. The mutated protein was then expressed and purified by the same procedures as used to obtain the WT protein.

Isothermal titration calorimetry

Calorimetric measurements were carried out using an MCS ITC-instrument from MicroCal Inc. (Northampton, USA). In each experiment, the ligand was titrated to the protein solution present in the 1.4 ml sample cell. The reference cell contained 0.1 mM sodium azide dissolved in demineralised water. All measurements were carried out at 298 K. In order to detect changes in the protonation state, all measurements were performed in phosphate, Hepes, Tricine, and Tris buffer. The corresponding buffer ionization enthalpies were taken from literature.[47,48] The WT protein was dissolved in a 10 mM solution of the appropriate buffer at pH 8 to a concentration of 18.9 μM for the titration of inhibitors **2, 3, 6,** and **8** and 37.8 μM for the measurements of inhibitors **4, 5,** and **7**. For the Y48F mutant, all measurements were performed with a protein concentration of 37.8 μM. Protein concentrations were determined by UV spectroscopy (280 nm) using the specific absorption calculated by the ProtParam tool‡.

‡ www.expasy.ch

The ligand solution contained 252 μM of the corresponding inhibitor dissolved in the same buffer as the protein. The protein was saturated with an excess of $NADP^+$, which was present at the same concentration in the ligand solution to avoid heat effects caused by diluting the cofactor. Solutions were degassed at 293 K under vacuum for 10 min. Upon experimental setup, the protein solution present in the sample cell was stirred at 400 rpm. After a stable baseline had been achieved, the titration was initiated. The injection sequence started with an initial aliquot of 1.5 μl (to preserve diffusion effects arising from the experimental setup; data not used for fitting) followed by injections of 10 μl in time intervals of 300 s until complete saturation was obtained. Heat changes caused by each inhibitor injection were obtained from the integral of the calorimetric signal. Data were analysed using the ORIGIN software (MicroCal Inc.) for fitting the data points to a single-site binding model in agreement with the results from X-ray crystallography.

Experimental heats of the protein–inhibitor titration were corrected for heats of dilution by subtracting the average heat of the last three measurements after saturation of the protein binding sites had been achieved. All measurements were carried out at least in duplicate. Energy values, binding constants, and standard deviations were derived from data fitting and subsequent averaging of the corresponding measurements. Standard Gibbs free energy values were calculated using the equation $\Delta G^0 = -RT \ln K_b$ (where $R = 8.3144$ J mol^{-1}K^{-1}, and K_b is binding constant). The determination of ΔH^0_{exp} was performed for inhibitors **2**–**6** using the linear regression of experimentally observed enthalpies and subsequent extrapolation towards the *y*-axis, whereas ΔH^0_{exp} for inhibitors **7** and **8** was calculated using the enthalpy value observed in Hepes buffer. For the determination of the ionization enthalpies of inhibitors **5** and **6** a 2 mM solution of each inhibitor in purified water was prepared and the pH adapted to the pK_a value of both compounds. This solution was titrated with 10 μl injections of 1 mM HCl. The corresponding ionization enthalpies were obtained by subtraction of the heats determined by a blank titration followed by subsequent averaging of the heats obtained from at least ten injection peaks. The ionization enthalpies observed (**5**: 28.3(±2.5) kJ mol^{-1}; **6**: 32.8(±3.1) kJ mol^{-1}) are in agreement with the corresponding value reported for the first ionization of an appropriate hydantoin analogue (32.6 kJ mol^{-1}).[49] The ligand binding enthalpy ΔH^0_{bind} was calculated using the experimental heat ΔH^0_{exp} according to equation (2). To obtain ΔH^0_{bind}, the ionization enthalpy of buffer, protein residue (tyrosine) and, if present, the ligand were subtracted from ΔH^0_{exp} using the coefficients given in Table 4.

pK_a determination

The crystal structures of ALR2 in complex with inhibitor **2** (IDD388), **3** (IDD393) and **4** have recently been determined in our laboratory.[23] The experimentally determined pK_a value of inhibitor **1** (IDD594) is 2.9.[11] The structural similarity of inhibitors **1**, **2**, and **3** tempted us to perform the pK_a calculations based on the pK_a value of inhibitor **1** for all carboxylate head groups. For the sake of consistency, a pK_a value of 3.0 was also assumed for inhibitor **4** in our calculations. However, changing the pK_a value by ±1 unit does not suggest different protonation effects. For the pK_a calculations, we applied the same methodology as recently described.[9] MEAD was employed as the PB solver.[24] We performed the calculations with a dielectric constant of 20 and 10 to elucidate its influence. REDUCE was used to generate hydrogen atoms for the residues of the protein.[50] For the calculations of the complexes, the orientation of the Tyr48 OH group was chosen to point towards the ligand. SYBYL was applied to add hydrogen atoms to the cofactor and the ligands§. To study the protonation effects upon ligand binding, two pK_a calculations are required: One without ligand and a second with the bound ligand. Only the titratable residues within a 12 Å sphere around the active site were selected for evaluation of the site–site interactions in order to reduce the computational effort (in total, there are 91 titratable residues in human ALR2). This results in the following 26 titratable residues: Lys21, Asp43, Cys44, His46, Tyr48, Glu51, Lys77, Cys80, Tyr82, His83, His110, Lys116, Lys119, Glu120, Glu185, Cys186, Tyr209, Asp216, Lys262, Cys298, Cys303, His306, Lys307, Asp308, Tyr309 and His312. We used the higher populated amino acid conformer in case a split conformation had been assigned in the crystal structure. In contrast to our standard settings for the titration of histidine residues, the N^{δ} atom of His110 was titrated.

pK_a values of inhibitors **2**–**6** were determined in an aqueous solution of 0.15 M KCl at 296 K using a photometric procedure. UV absorption spectra were recorded using a Perkin-Elmer Spectrophotometer Lambda 7 with 1 cm path-length. A series of 20 buffer solutions in the range of pH1.5 to 10.9 was prepared using KCl/HCl and phosphate salts of analytical grade. Equal amounts of a ligand stock solution were diluted by the appropriate buffer solution for subsequent absorbance measurements. The absorbance was plotted against pH and pK_a values were determined by analysis of the photometric titration curves. Figures were prepared using Isis Draw (MDL, San Leandro, USA) and PyMOL‖. Calculations of the solvent-accessible surface buried upon complex formation were performed with the web-accessible tool GETAREA 1.1[51] using a 1.4 Å probe and radii published by Shrake & Rupley.[52]

Acknowledgements

We thank Dr Alberto Podjarny, IGBMC, Illkirch, France for providing us with the expression clone of human ALR2 and with test compounds (**2**,**3**,**6** and **8**). Sorbinil (**5**) was kindly provided by Pfizer, Inc., Connecticut. We thank Diana Fladerer, Philipps-University Marburg for technical assistance in preparation of the mutant enzyme. The bilateral financial support of CNRS and DFG under the CERC3 program (KL1204/3, KL1204/4) as well as the Graduiertenkolleg "Protein function at the atomic level" is gratefully acknowledged.

References

1. Homans, S. W. (2005). Probing the binding entropy of ligand protein interactions by NMR. *ChemBioChem.* **6**, 1–8.

§ SYBYL 6.6, Tripos, Inc., Missouri, USA.

‖ DeLano, W. L. (2002). The PyMOL Molecular Graphics System. (http://www.pymol.org).

2. Ladbury, J. E. & Ababou, A. (2005). Survey of the year 2004: literature on applications of isothermal titration calorimetry. *J. Mol. Recognit.* **1**, 79–89.
3. Holdgate, G. A. & Ward, W. H. J. (2005). Measurements of binding thermodynamics in drug discovery. *Drug Discov. Today*, **10**, 1543–1550.
4. Ruben, A. J., Kiso, Y. & Freire, E. (2006). Overcoming roadblocks in lead optimization: a thermodynamic perspective. *Chem. Biol. Drug Res.* **67**, 2–4.
5. Dullweber, F., Stubbs, M. T., Musil, D., Stürzebecher, J. & Klebe, G. (2001). Factorizing ligand affinity: a combined thermodynamic and crystallographic study of trypsin and thrombin inhibition. *J. Mol. Biol.* **313**, 593–614.
6. Velazquez-Campoy, A., Todd, M. J. & Freire, E. (2000). HIV-1 protease inhibitors: enthalpic versus entropic optimization of the binding affinity. *Biochemistry*, **39**, 2201–2207.
7. Velazquez-Campoy, A., Kiso, Y. & Freire, E. (2001). The binding energetics of first- and second-generation HIV-1 protease inhibitors: implications for drug design. *Arch. Biochem. Biophys.* **390**, 169–175.
8. Warshel, A., Sharma, P. K., Kato, M. & Parson, W. W. (2006). Modeling electrostatic effects in proteins. *BBA – Proteins Proteom.* **1764**, 1647–1676.
9. Czodrowski, P., Dramburg, I., Sotriffer, C. A. & Klebe, G. (2006). Development, validation and application of adapted PEOE charges to estimate p*K*(a) values of functional groups in protein-ligand complexes. *Proteins: Struct. Funct. Genet.* **65**, 424–437.
10. Baker, B. M. & Murphy, K. P. (1996). Evaluation of linked protonation effects in protein binding reactions using isothermal titration calorimetry. *Biophys. J.* **71**, 2049–2055.
11. Howard, E. I., Sanishvili, R., Cachau, R. E., Mitschler, A., Chevrier, B., Barth, P. *et al.* (2004). Ultrahigh resolution drug design I: details of interactions in human aldose reductase-inhibitor complex at 0.66 Å. *Proteins: Struct. Funct. Genet.* **55**, 792–804.
12. El-Kabbani, O., Wilson, D. K., Petrash, J. M. & Quiocho, F. A. (1998). Structural features of the aldose reductase and aldehyde reductase inhibitor binding sites. *Mol. Vis.* **4**, 19–25.
13. Urzhumtsev, A., Tete-Favier, F., Mitschler, A., Barbanton, J., Barth, P., Urzhumtseva, L. *et al.* (1997). A 'specificity' pocket inferred from the crystal structures of the complexes of aldose reductase with the pharmaceutically important inhibitors tolrestat and sorbinil. *Structure*, **5**, 601–612.
14. Steuber, H., Zentgraf, M., Podjarny, A. D., Heine, A. & Klebe, G. (2006). High resolution crystal structure of aldose reductase complexed with the novel sulfonylpyridazinone inhibitor exhibiting an alternative active site anchoring group. *J. Mol. Biol.* **356**, 45–56.
15. Varnai, P., Richards, W. & Lyne, P. D. (1999). Modelling the catalytic reaction in human aldose reductase. *Proteins: Struct. Funct. Genet.* **37**, 218–227.
16. Cachau, R., Howard, E., Barth, P., Mitschler, A., Chevrier, B., Lamour, V. *et al.* (2000). Model of the catalytic mechanism of human aldose reductase based on quantum chemical calculations. *J. Phys. IV France*, **10**, 3–13.
17. Brownlee, M. (2001). Biochemistry and molecular cell biology of diabetic complications. *Nature*, **414**, 813–820.
18. Evans, J. L., Goldfine, I. D., Maddux, B. A. & Grodsky, G. M. (2002). Oxidative stress and stress-activated signalling pathways: a unifying hypothesis of type 2 diabetes. *Endocrine Rev.* **23**, 599–622.
19. Price, S. A., Agthong, S., Middlemas, A. B. & Tomlinson, D. R. (2004). Mitogen-activated protein kinase p38 mediates reduced nerve conduction velocity in experimental diabetic neuropathy. Interactions with aldose reductase. *Diabetes*, **53**, 1851–1856.
20. Suzuki, L. A., Poot, M., Gerrity, R. G. & Bornfeldt, K. E. (2001). Diabetes accelerates smoth muscle accumulation in lesions of atherosclerosis. Lack of direct growth-promoting effects of high glucose levels. *Diabetes*, **50**, 851–860.
21. Nakamura, J., Kasuya, Y., Hamada, Y., Nakashima, E., Naruse, K., Yasuda, Y. *et al.* (2001). Glucose-induced hyperproliferation of cultured rat aortic smooth muscle cells through polyol pathway hyperactivity. *Diabetologica*, **44**, 480–487.
22. Krämer, O., Hazemann, I., Pojarny, A. D. & Klebe, G. (2004). Virtual screening for inhibitors of human aldose reductase. *Proteins: Struct. Funct. Genet.* **55**, 814–823.
23. Steuber, H., Heine, A. & Klebe, G. (2007). Structural and thermodynamic characterization of aldose reductase inhibitors reveals a nitro-substituent as strong enthalpic contributor to ligand affinity. *J. Mol. Biol.* **368**, 618–638.
24. Bashford, D. (1997). An object-oriented programming suite for electrostatic effects in biological molecules. In *Lecture Notes in Computer Science* (Ishikawa, Y., Oldehoeft, R. R., Reynders, J. V. W. & Tholburn, M., eds), pp. 233–240, Springer, Berlin.
25. Czodrowski, P., Sotriffer, C. A. & Klebe, G. (2007). Protonation changes upon ligand binding to trypsin and thrombin: structural interpretation based on pK_a calculations and ITC experiments. *J. Mol. Biol.* **367**, 1347–1356.
26. Czodrowski, P., Sotriffer, C. A. & Klebe, G. (2007). Atypical protonation states in the active site of HIV-1 protease: A computational study. *J. Chem. Inf. Model.* **47**, 1590–1598.
27. Baker, N. A. (2005). Biomolecular applications of Poisson-Boltzmann methods. In *Reviews in Computational Chemistry* (Lipkowitz, K. B., Larter, R. & Cundari, T. R., eds), John Wiley and Sons, Hoboken, NJ.
28. Schutz, C. N. & Warshel, A. (2001). What are the dielectric "constants" of proteins and how to validate electrostatic models? *Proteins: Struct. Funct. Genet.* **44**, 400–417.
29. Antosiewicz, J., McCammon, J. A. & Gilson, M. K. (1994). Prediction of pH-dependent properties of proteins. *J. Mol. Biol.* **238**, 415–436.
30. Demchuk, E. & Wade, R. C. (1996). Improving the continuum dielectric approach to calculating pK_as of ionizable groups in proteins. *J. Phys. Chem.* **100**, 17373–17387.
31. Nielsen, J. E. & McCammon, J. A. (2003). Calculating pK_a values in enzyme active sites. *Protein Sci.* **12**, 1894–1901.
32. Tarle, I., Borhani, D. W., Wilson, D. K., Quiocho, F. A. & Petrash, J. M. (1993). Probing the active site of human aldose reductase. *J. Biol. Chem.* **268**, 25687–25693.
33. Grimshaw, C. E., Bohren, K. M., Lai, C.-J. & Gabbay, K. H. (1995). Human aldose reductase: p*K* of tyrosine 48 reveals the preferred ionization state for catalysis and inhibition. *Biochemistry*, **34**, 14374–14384.
34. Gerratana, B., Cleland, W. W. & Frey, P. A. (2001). Mechanistic roles of Thr134, Tyr160, and Lys164 in the reaction catalyzed by dTDP-glucose 4,6-dehydratase. *Biochemistry*, **40**, 9187–9195.

35. Liu, Y., Thoden, J. B., Kim, J., Berger, E., Gulick, A. M., Ruzicka, F. J. *et al.* (1997). Mechanistic roles of tyrosine 149 and serine 124 in UDP-galactose 4-epimerase from *Escherichia coli*. *Biochemistry*, **36**, 10675–10684.
36. Gustafsson, A., Etahadieh, M., Jemth, P. & Mannervik, B. (1999). The C-terminal region of human glutathione transferase A1-1 affects the rate of glutathione binding and the ionization of the active-site Tyr9. *Biochemistry*, **38**, 16268–16275.
37. Williams, M. A. & Ladbury, J. E. (2003). Hydrogen bonds in protein-ligand complexes. In *Protein–Ligand Interactions: From Molecular Recognition to Drug Design* (Boehm, H.-J. & Schneider, G., eds), pp. 137–161, Wiley-VCH, Weinheim.
38. Meot-Ner, M. (2005). The ionic hydrogen bond. *Chem. Rev.* **105**, 213–284.
39. Meyer, E. A., Castellano, R. K. & Diederich, F. (2003). Interactions with aromatic rings in chemical and biological recognition. *Angew. Chem. Int. Ed.* **42**, 1210–1250.
40. El-Kabbani, O., Darmanin, C., Schneider, T. R., Hazemann, I., Ruiz, F., Oka, M. *et al.* (2004). Ultrahigh resolution drug design. II. Atomic resolution structures of human aldose reductase holoenzyme complexed with fidarestat and minalrestat: implications for the binding of cyclic imide inhibitors. *Proteins: Struct. Funct. Genet.* **55**, 805–813.
41. Petrova, T., Steuber, H., Hazemann, I., Cousido-Siah, A., Mitschler, A., Chung, R. *et al.* (2005). Factorizing selectivity determinants of inhibitor binding toward aldose and aldehyde reductases: structural and thermodynamic properties of the aldose reductase mutant Leu300Pro-fidarestat complex. *J. Med. Chem.* **48**, 5659–5665.
42. Blakeley, M. P., Mitschler, A., Hazemann, I., Meilleur, F., Myles, D. A. & Podjarny, A. (2006). Comparison of hydrogen determination with X-ray and neutron crystallography in a human aldose reductase-inhibitor complex. *Eur. Biophys. J.* **35**, 577–583.
43. Baker, B. M. & Muphy, K. P. (1997). Dissecting the energetics of a protein–protein interaction: the binding of ovomucoid third domain to elastase. *J. Mol. Biol.* **268**, 557–569.
44. Xie, D., Gulnik, S., Collins, L., Gustchina, E., Suvorov, L. & Erickson, J. W. (1997). Dissection of the pH dependence of inhibitor binding energetics for an aspartic protease: direct measurement of the protonation states of the catalytic aspartic acid residues. *Biochemistry*, **36**, 16166–16172.
45. Gomez, J. & Freire, E. (1995). Thermodynamic mapping of the inhibitor site of the aspartic protease endothiapepsin. *J. Mol. Biol.* **252**, 337–350.
46. Sotriffer, C. A., Krämer, O. & Klebe, G. (2004). Probing flexibility and "induced-fit" phenomena in aldose reductase by comparative crystal structure analysis and molecular dynamics simulations. *Proteins: Struct. Funct. Genet.* **56**, 52–66.
47. Fukada, H. & Takahashi, K. (1998). Enthalpy and heat capacity changes for the proton dissociations of various buffer components in 0.1 M potassium chloride. *Proteins: Struct. Funct. Genet.* **33**, 159–166.
48. Christensen, J. J., Hansen, L. D. & Izatt, R. M. (1976). *Handbook of Proton Ionization Heats and Related Thermodynamic Quantities.* Wiley, New York.
49. Lennette, E. P. & Plapp, B. V. (1979). Kinetics of carboxymethylation of histidine hydantoin. *Biochemistry*, **18**, 3933–3938.
50. Word, J. M., Lovell, S. C., Richardson, J. S. & Richardson, D. C. (1999). Asparagine and glutamine: using hydrogen atom contacts in the choice of side-chain amide orientation. *J. Mol. Biol.* **285**, 1735–1747.
51. Fraczkiewicz, R. & Braun, W. (1998). Exact and efficient analytical calculation of the accessible surface areas and their gradients for macromolecules. *J. Comp. Chem.* **19**, 319–333.
52. Shrake, A. & Rupley, J. A. (1973). Environment and exposure to solvent of protein atoms. Lysozyme and insulin. *J. Mol. Biol.* **79**, 351–371.